Supporting Information

Rationally-Designed PdAuCu Ternary Alloy Nanoparticles for Intrinsically Deactivation-Resistant Ultrafast Plasmonic Hydrogen Sensing

Iwan Darmadi[1, ‡], Ferry Anggoro Ardy Nugroho[1, ‡], Shima Kadkhodazadeh[2], Jakob B. Wagner[2] and Christoph Langhammer[1]*

[1]Department of Physics, Chalmers University of Technology, 412 96 Göteborg, Sweden

[2]Center for Electron Nanoscopy, Technical University of Denmark, 2800 Kongens Lyngby, Denmark

1. Electron Microcopy Images and Elemental Maps of PdCu Alloys

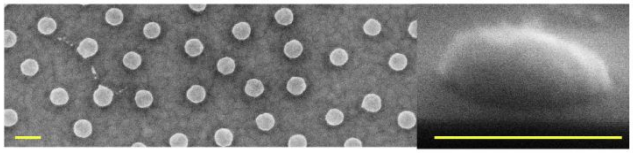

Figure S1. *Left panel: overview SEM image of an alloyed $Pd_{85}Cu_{15}$ nanodisk array. Right panel: 70°-tilt SEM image of a single $Pd_{85}Cu_{15}$ nanodisk. Scale bars: 200 nm.*

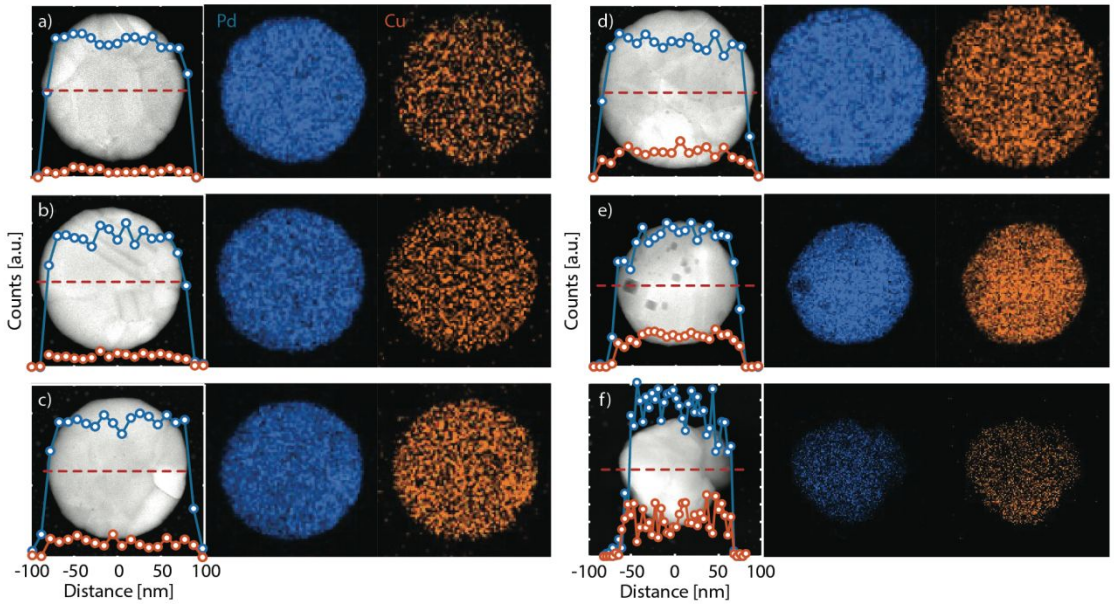

Figure S2. *STEM image of a single nanodisk together with EDS elemental linescans along the red dashed-line (left) and the corresponding elemental maps (right) of (a) $Pd_{95}Cu_5$ (b) $Pd_{90}Cu_{10}$ (c) $Pd_{85}Cu_{15}$ (d) $Pd_{80}Cu_{20}$ (e) $Pd_{75}Cu_{25}$ and (f) $Pd_{70}Cu_{30}$.*

2. Optical Properties of PdCu Alloy Nanoparticles with Different Composition

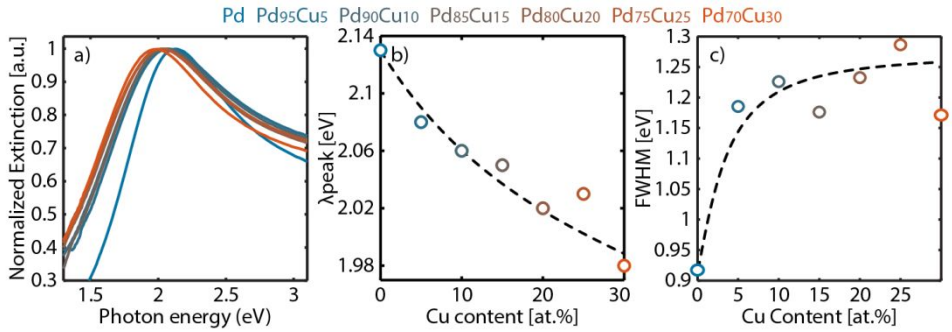

Figure S3. *(a) Normalized optical extinction spectra of PdCu alloy nanoparticle arrays with different composition. (b) LSPR peak, λ_{peak}, and (c) full-width at half maximum (FWHM) of the plasmon resonance peak plotted as a function of Cu content in the alloy. The FWHM is defined as the peak half-width, as measured from the λ_{peak} toward the low energy side, multiplied by two, to exclude possible contributions by higher order plasmonic modes. Smooth transition of λ_{peak} and FWHM as function of Cu content indicates formation of homogeneous alloys. The dashed lines serve as a guide to the eye.*

3. Simultaneous Plasmonic and Quartz Crystal Microbalance Measurements

To correlate the optical properties of PdCu nanoparticles with the hydrogen concentration inside them we employed simultaneous nanoplasmonic and QCM measurements from the same sample surface[1] (**Figure S4**). To this end, we used optical measurements in reflectance mode to record the optical change in the nanoparticles upon exposure to different hydrogen partial pressures and simultaneously, *via* the resonance frequency shift, Δf, of the QCM crystal and the Sauerbrey equation,[2] determine the absolute amount of hydrogen absorbed by the nanoparticles. From ref. S1 it has been determined that for nanoparticles with a height of 25 nm, as the case here, the hydrogen concentration in them can be expressed as

$$\Delta H/Pd = 1.70E^{-2\frac{\Delta f}{\alpha\beta}} \quad \text{(S1)}$$

where α and β are the Pd content in the alloy and the nanoparticle surface coverage, respectively. To this end the coverage β should be identified carefully for each sample since it is expected to vary from sample to sample. We examined the coverage by SEM and systematically mapped different locations on the QCM crystal to get good statistics from an area of a total of 160 μm^2. The corresponding results are summarized in **Table S1**.

Table S1. α and β Parameters for PdCu Alloy Systems Considered

Sample	α	β [%]
Pd	1.00	11.9
$Pd_{95}Cu_5$	0.95	12.9
$Pd_{90}Cu_{10}$	0.90	11.5
$Pd_{85}Cu_{15}$	0.85	14.6
$Pd_{80}Cu_{20}$	0.80	16.5
$Pd_{75}Cu_{25}$	0.75	14.8
$Pd_{70}Cu_{30}$	0.70	15.1

Using equation S1 we then constructed the gravimetric QCM-based isotherms (expressed as hydrogen-palladium atomic ratio, *H/Pd*) of all the investigated PdCu alloy nanoparticle arrays, plotted together with the simultaneously obtained optical ones in **Figure S5**. A remarkable similarity between the optical and gravimetric isotherms is observed for each PdCu system. From these data we also obtained the hydrogen concentration in the different alloys at 250 mbar plotted in **Figure S6**. The overall trend of a linearly decreasing *H/Pd*, as well as the absolute *H/Pd* values, are in excellent agreement with reports for bulk PdCu alloys.[3]

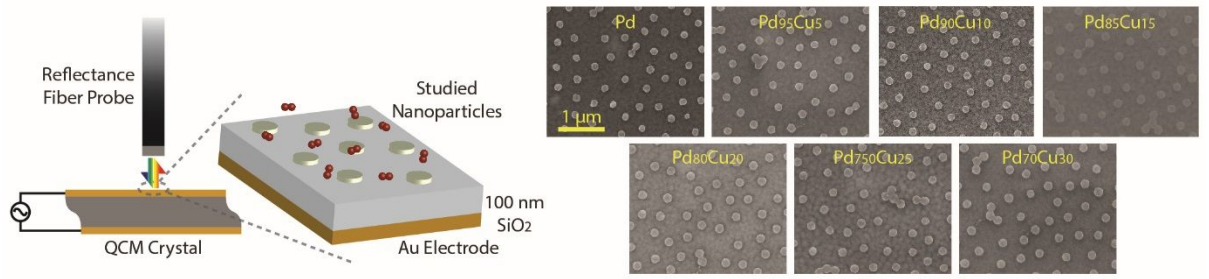

Figure S4. *Left: schematic representation of the combined QCM and optical readout setup, where the latter is implemented in reflection mode via a fiber optic reflectance probe connected to a white light source and a fixed-grating spectrometer. To minimize coupling of the LSPR modes in the investigated nanoparticles with the Au electrode of the QCM crystal, a 100-nm thick SiO_2 spacer layer is grown on the QCM electrode, onto which the nanoparticles subsequently are fabricated. The schematic is adapted with permission from ref. S1. Copyright 2018 American Chemical Society. Right: SEM images of different PdCu alloy nanoparticle arrays fabricated on QCM crystals.*

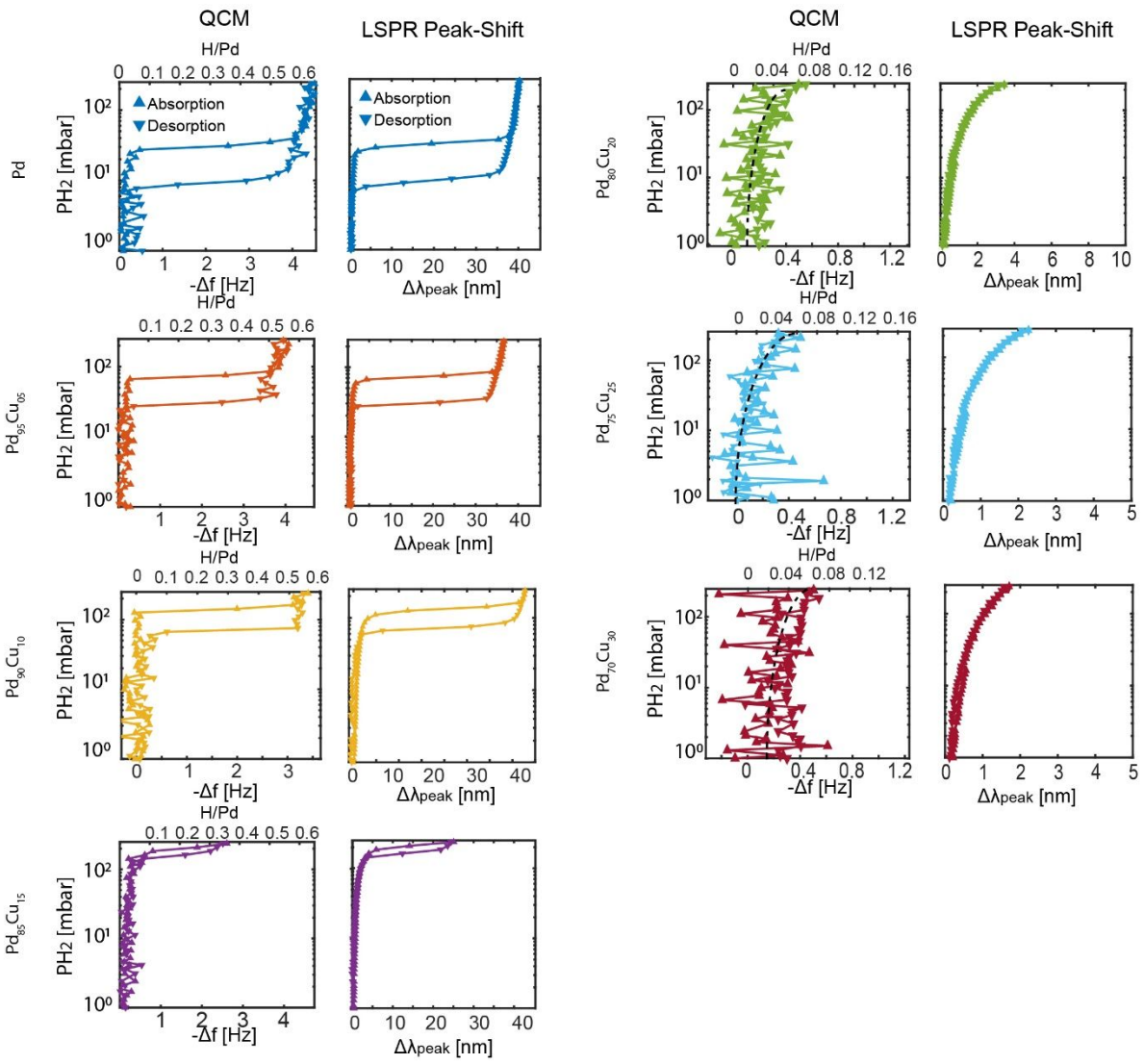

Figure S5. *Simultaneously measured gravimetric (QCM) and optical (LSPR) hydrogen absorption and desorption isotherms for PdCu alloy nanoparticles with different composition, measured at 303 K. Note that for PdCu alloys with Cu content > 15 at.% the nanoparticles remain in the α-phase at 250 mbar. The upward and downward triangles denote the hydrogen absorption and desorption branches of the isotherm, respectively. The data of Pd-$Pd_{75}Cu_{25}$ is adapted with permission from ref. S1. Copyright 2018 American Chemical Society.*

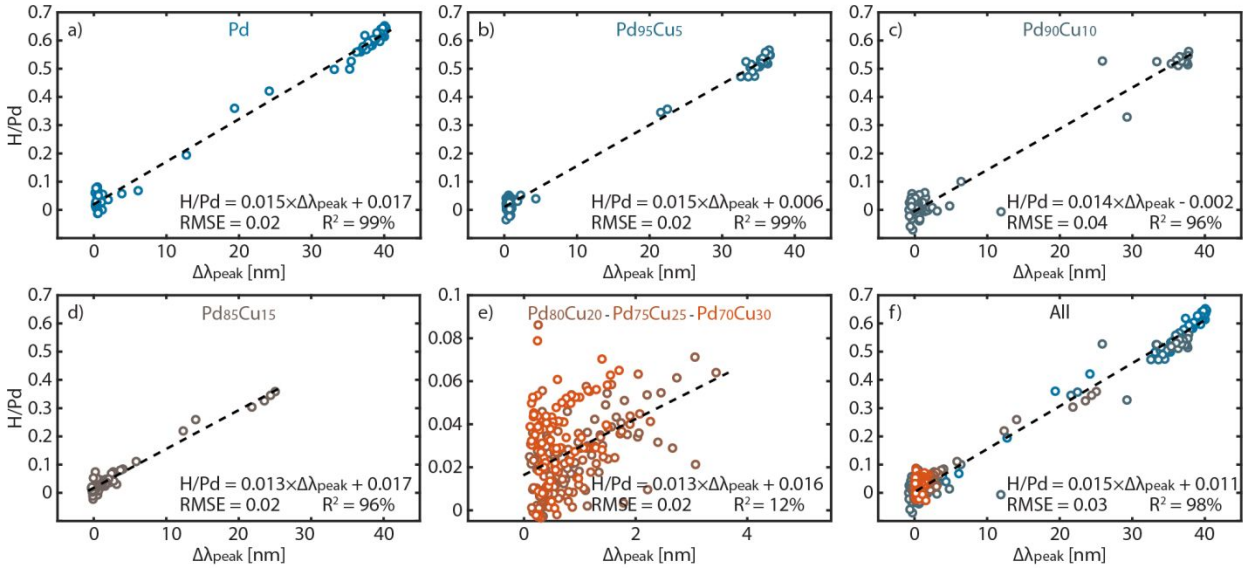

Figure S6. *Correlation between the optical readout parameter $\Delta\lambda_{peak}$ and relative hydrogen concentration in Pd and PdCu alloy nanoparticles. $\Delta\lambda_{peak}$-H/Pd correlation plots for (a) Pd, (b) $Pd_{95}Cu_5$, (c) $Pd_{90}Cu_{10}$, (d) $Pd_{85}Cu_{15}$, (e) $Pd_{80}Au_{20}$, $Pd_{75}Au_{25}$, and $Pd_{70}Au_{30}$. Linear regression (dashed lines) is applied to describe the $\Delta\lambda_{peak}$-H/Pd relation and shown together with corresponding root-mean-square error (RMSE) and R^2 values. Note how all the systems exhibit similar slopes and thus identical scaling with the hydrogen concentration in the nanoparticles expressed as H/Pd. This becomes obvious in the master plot (f) where data for all the different alloy compositions are plotted together. The experiments were carried out at atmospheric pressure using Ar as carrier gas. The data of Pd-$Pd_{75}Cu_{25}$ is adapted with permission from ref. S1. Copyright 2018 American Chemical Society.*

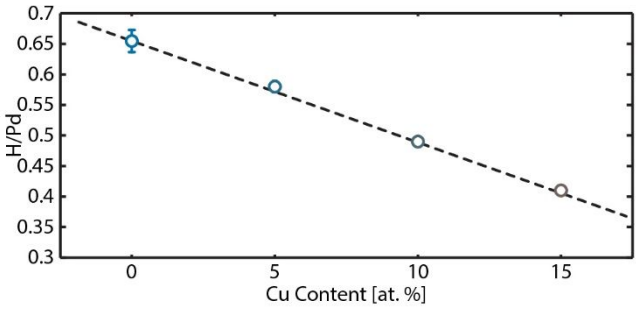

Figure S7. *Absolute hydrogen concentration, expressed as H/Pd, in PdCu alloy nanoparticles with different composition measured at 250 mbar hydrogen partial pressure in Ar carrier gas and at 30 ˚C. Note that the H/Pd ratio for PdCu with Cu content beyond 15 at.% is not available since these samples do not transform into the hydride–phase at 250 mbar at 30 ˚C (see* ***Figure S5****). The overall trend of a linearly decreasing H/Pd, as well as the absolute values, are in excellent*

agreement with reports of bulk PdCu alloys.[3] The error bars denote the standard deviation from at least three measurements. The dashed line is a guide to the eye.

4. Extinction Spectra Upon Hydrogen Sorption

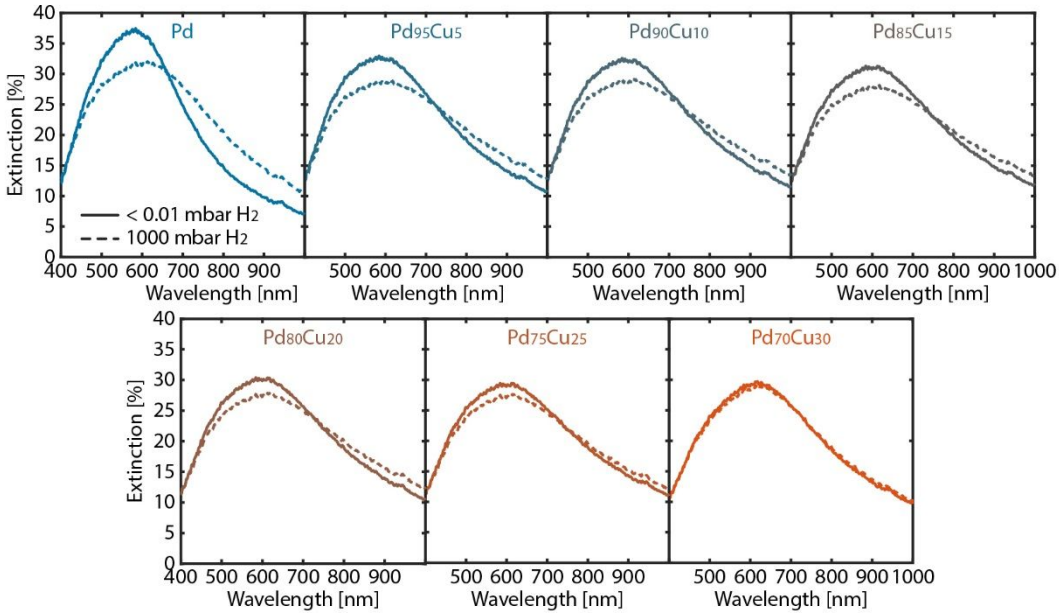

Figure S8. *Optical extinction spectra of the different PdCu alloy nanoparticles upon exposure to <0.01 mbar (solid lines) and 1000 mbar (dashed lines) hydrogen, measured in a vacuum chamber.*

5. $Pd_{70}Cu_{30}$ Deactivation Test

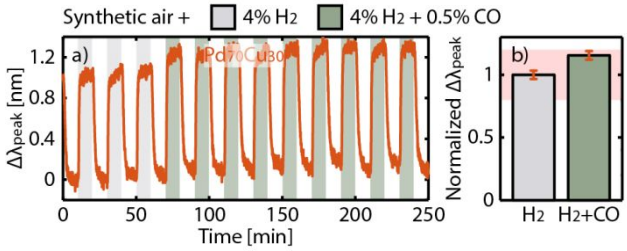

Figure S9. *(a) Time-dependent $\Delta\lambda_{peak}$ response of $Pd_{70}Cu_{30}$ to three 10-min 4% H_2 pulses (grey shaded areas) followed by 9 pulses of 4% H_2 + 0.5% CO mixture (green shaded areas) measured at atmospheric pressure at a constant flow rate of 100 mL/min. (b) $\Delta\lambda_{peak}$ response in CO background normalized to the one obtained in pure 4% H_2. The error bars denote the standard deviation from 10 cycles. The red shaded areas indicate the ±20% deviation limit from the normalized $\Delta\lambda_{peak}$ in pure 4% H_2 according to the performance standard for hydrogen sensors.*[4]

6. Determination of Experimental λ_{peak} and Noise

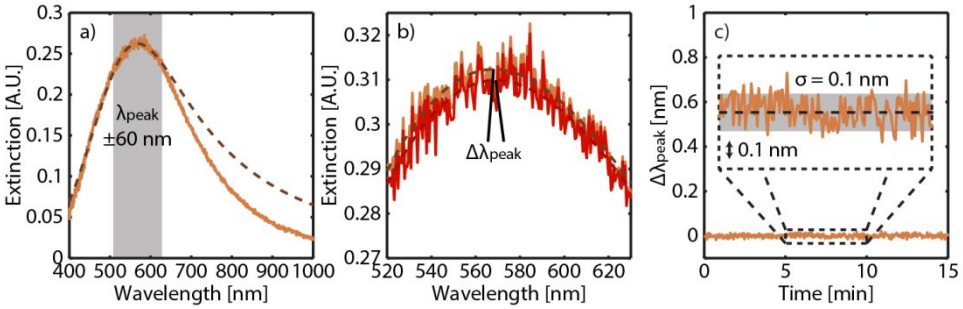

Figure S10. *(a) Lorentzian function fitting to the optical spectra of $Pd_{70}Au_{25}Cu_5$ sensor. The fit (dashed line) is only applied within ±60 nm from the λ_{peak} (shared area) where it is symmetric and thus provides a good fit with $R^2 > 0.96$,(b) Example of $\Delta\lambda_{peak}$ determination of the sensor from vacuum (orange line) to 5 mbar H_2 (red). Using the fitting, in this case, $\Delta\lambda_{peak}$ of 1 nm can be resolved. (c) Typical signal noise obtained using the fitting procedure. The data show $\Delta\lambda_{peak}$ of a sensor in vacuum for 15 min. Clearly a stable signal is achieved with determined noise, σ, of 0.1 nm (shaded area in the inset).*

7. $\Delta\lambda_{peak}$ Response in Low Hydrogen Concentration

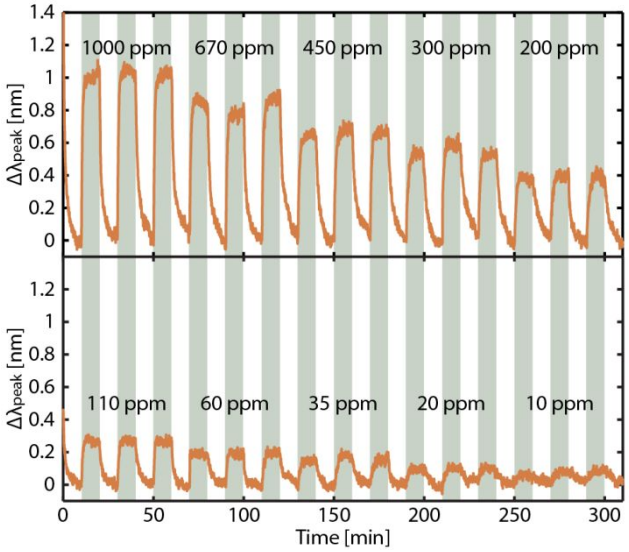

Figure S11. *Time-resolved $\Delta\lambda_{peak}$ response of the $Pd_{70}Au_{25}Cu_5$ ternary alloy sensor to different hydrogen concentrations in Ar measured at 30 °C in flow mode. Shaded areas denote exposure to hydrogen.*

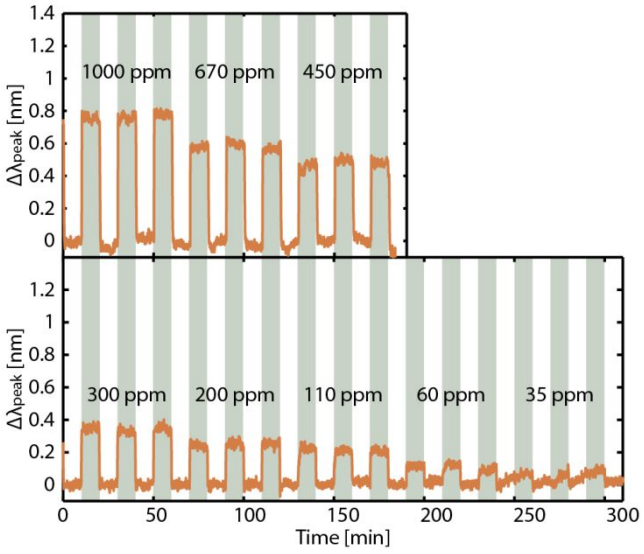

Figure S12. *Time-resolved $\Delta\lambda_{peak}$ response of the $Pd_{70}Au_{25}Cu_5$ ternary alloy sensor to different hydrogen concentrations in synthetic air measured at 30 °C in flow mode. Shaded areas denote exposure to hydrogen.*

8. $Pd_{70}Au_{25}Cu_5$ Alloy Nanoparticles Resistance Towards CO at Lower H_2 Pressure

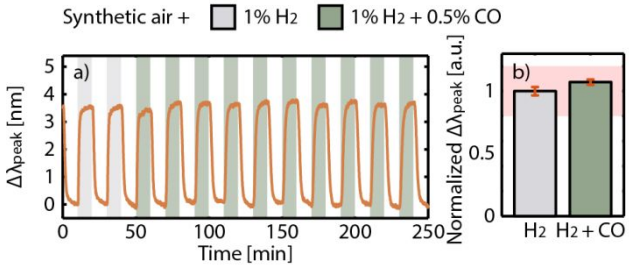

Figure S13. *Time-resolved $\Delta\lambda_{peak}$ response of $Pd_{70}Au_{25}Cu_5$ to two 1% H_2 pulses (grey shaded areas) followed by (a) 10 pulses of 1% H_2 + 0.5% CO_2 (green shaded areas). (b) The corresponding normalized $\Delta\lambda_{peak}$ responses to 1% H_2 in synthetic air with CO background, with respect to the control response in pure 1% H_2 in synthetic air. The error bars denote the standard deviation from 10 cycles. The red shaded areas indicate the ±20% deviation limit from the normalized $\Delta\lambda_{peak}$ in pure 4% H_2 according to the performance standard for hydrogen sensors.*[4]

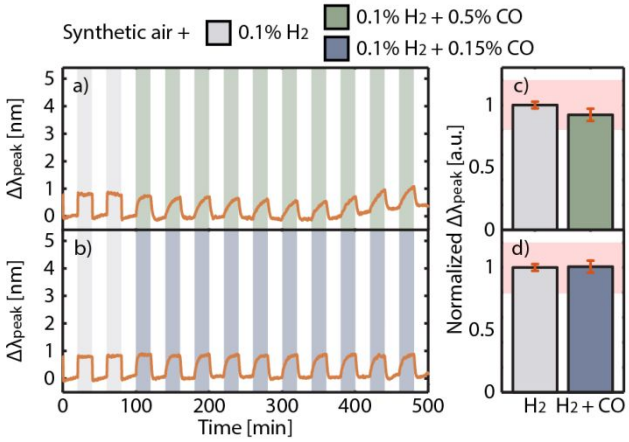

Figure S14. *Time-resolved $\Delta\lambda_{peak}$ response of $Pd_{70}Au_{25}Cu_5$ to two 0.1% H_2 pulses (grey shaded areas) followed by (a) 10 pulses of 0.1% H_2 + 0.5% CO_2 (green shaded areas) or (b) 10 pulses of 0.1% H_2 + 0.15% CH_4 (blue shaded areas), all in synthetic air carrier gas. The corresponding normalized $\Delta\lambda_{peak}$ responses to 0.1% H_2 in synthetic air with (c) 0.5% and (d) 0.15% CO backgrounds, with respect to the control response in pure 0.1% H_2 in synthetic air. The error bars denote the standard deviation from 10 cycles. The red shaded areas indicate the ±20% deviation limit from the normalized $\Delta\lambda_{peak}$ in pure 4% H_2 according to the performance standard for hydrogen sensors.*[4] *Note that the response kinetics of the sensor exposed to 0.5% CO are slower than for 0.15%, which mainly is responsible for the lower $\Delta\lambda_{peak}$ observed within the CO-exposure period.*

9. $Pd_{70}Au_{25}Cu_5$ Alloy Nanoparticles Resistance Towards CO_2 and CH_4

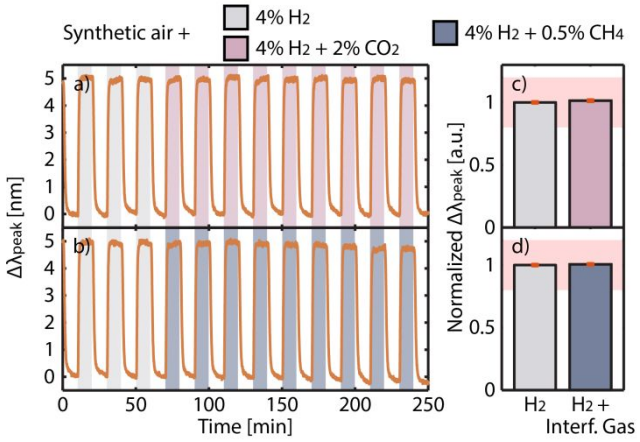

Figure S15. *Time-resolved $\Delta\lambda_{peak}$ response of $Pd_{70}Au_{25}Cu_5$ to three 4% H_2 pulses (grey shaded areas) followed by (a) 9 pulses of 4% H_2 + 2% CO_2 (pink shaded areas) or (b) 9 pulses of 4% H_2 + 0.5% CH_4 (blue shaded areas), all in synthetic air carrier gas. The corresponding normalized $\Delta\lambda_{peak}$ responses to 4% H_2 in synthetic air with CO_2 (c) and CH_4 (d) backgrounds, with respect to the control response in pure 4% H_2 in synthetic air. The error bars denote the standard deviation from 10 cycles. The red shaded areas indicate the ±20% deviation limit from the normalized $\Delta\lambda_{peak}$ in pure 4% H_2 according to the performance standard for hydrogen sensors.*[4]

10. $Pd_{70}Au_{25}Cu_5$ Alloy Nanoparticles Stability Over Time

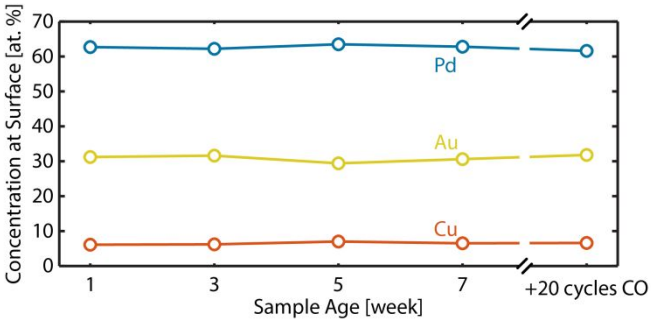

Figure S16. *Temporal evolution of the elemental composition at the alloy nanoparticle surface determined by XPS. Note that the surface is slightly Au and Cu enriched with respect to the nominal bulk composition already directly after fabrication but then remains stable over the 7-week test period.*

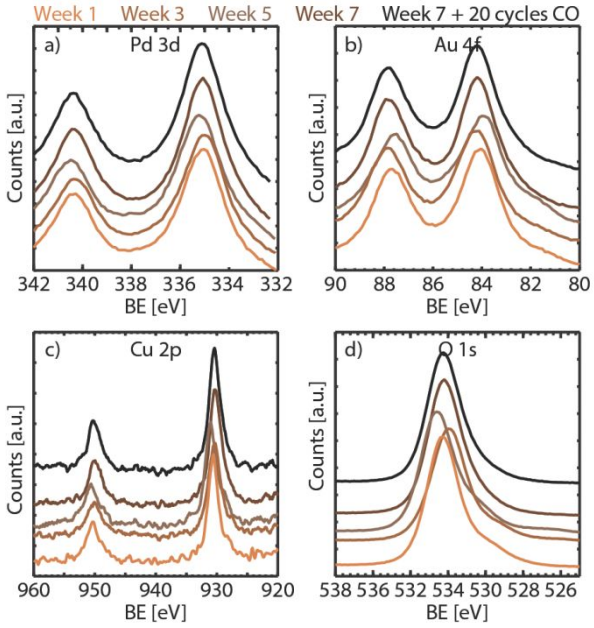

Figure S17. *XPS spectra showing the (a) Pd 3d, (b) Au 4f, (c) Cu 2p and (d) O 1s peaks measured on a $Pd_{70}Au_{25}Cu_5$ alloy sample during a 7 week period, including after exposure to CO in week 7. Note the generally high stability of the sample surface and, particularly that there neither is any sign of surface segregation of an alloyant over time, nor of oxidation due to the complete absence of a CuO peak around 940 eV.*

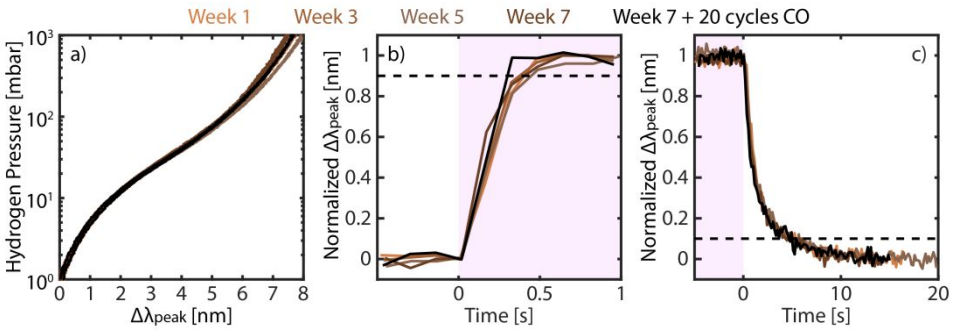

Figure S18. *(a) Hydrogen pressure-$\Delta\lambda_{peak}$ isotherms of the $Pd_{70}Au_{25}Cu_5$ alloy sample measured during a 7-week period, when stored at controlled ambient conditions (average temperature 21.2 °C, humidity 23% RH, and CO2 323 ppm). Note how the isotherms are basically unaffected, maintaining hysteresis-free response. (b) Absorption and (c) desorption kinetics measured during the same 7-week period. Again, the responses are very similar, retaining the initial response times of ca. 0.4 s and 5 s for absorption and desorption, respectively. The dashed lines in (c) and (d) mark the 90% and 10% of the maximum response, respectively. The red-shaded areas denote 40 mbar H_2 pulses.*

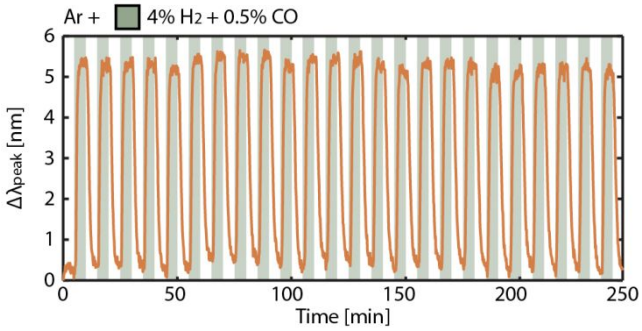

Figure S19. *Time-resolved $\Delta\lambda_{peak}$ response of a 7-week old $Pd_{70}Au_{25}Cu_5$ alloy sensor to 20 cycles of 4% H_2 + 0.5% CO in Ar carrier gas, measured at 30 °C.*

Table S2. Sensing metrics of state-of-the-art hydrogen sensors from the literature.

Active Element[a]	Transducing Method	t_{90} (s)	t_{10} (s)	Pressure[b] (mbar)	Temperature[b] (°C)	LoD (ppm)	Hysteretic Behaviour[c]	Resistance to Poisoning Gases[c]	Ref
PdAuCu NP	optical	0.4	5	40	RT	5	hysteresis-free	CO_2, CH_4, CO	this work
PdAu NP @PTFE@PMMA	optical	0.3	3	40	RT	1	hysteresis-free	CO_2, CH_4, CO, NO_2	[5]
Pd ultrasmall grain	electrical	12	19	30	RT	2.5	n.a.	n.a.	[6]
Pd strip on 3D structures	optical	20	-	1	RT	10	n.a.	n.a.	[7]
CeO_2-loaded In_2O_3 hollow spheres	electrical	24.5	21	0.05	160	0.01	n.a.	n.a.	[8]
Pd NW/ZnO	electrical	50	-	0.1	100	100	n.a.	n.a.	[9]
Pd NP/C NW	electrical	45	5	1	RT	10	n.a.	n.a.	[10]
Pd-SnO_2/MoS_2	electrical	26	15	1	RT	30	n.a.	n.a.	[11]
α-MoO_3 NW	electrical	3	2.7	15	260	100	n.a.	n.a.	[12]
Pd/SiC NCf	electrical	4	48	0.5	300	2	n.a.	n.a.	[13]
SiO_2 NR@Pd	electrical	17	-	10	RT	10	n.a.	n.a.	[14]
PdAg NW	electrical	120	102	1	RT	100	n.a.	n.a.	[15]
PdCuSi	mechanical	5	-	30	-	-	hysteresis-free	n.a.	[16]
Pt /YSZ/$LaSrCrFeO_3$-δ	electrical	4	24	1	450	20	n.a.	n.a.	[17]
Pd NC/TiO_2 NF	electrical	25	1	6	150	6000	n.a.	n.a.	[18]
MoS_2	electrical	14	140	10	30	-	n.a.	n.a.	[19]
Pd-capped Mg film	electrical	6	33	10	RT	1	n.a.	n.a.	[20]

Active Element[a]	Transducing Method	t_{90} (s)	t_{10} (s)	Pressure (mbar)	Temperature (^{o}C)	LoD (ppm)	Hysteretic Behaviour[b]	Resistance to Poisoning Gases[b]	Ref
UV-activated ZnO	electrical	4	24	10	RT	5	n.a.	n.a.	21
Pd NW@ZIF-8	electrical	13	6	1	RT	1000	n.a.	n.a.	22
Pd-Pt/ZnO NR	electrical	5	76	10	100	0.2	n.a.	n.a.	23
Pd NP/TiO2	electrical	12	5	1	180	1	n.a.	n.a.	24
Pd NP/MnO_2	electrical	30	40	1	100	10	n.a.	n.a.	25
Pt-TiO_2	electrical	10	20	1	RT	30	n.a.	n.a.	26
Pd NP/ZnO NR	electrical	100	-	5	RT	10	n.a.	n.a.	27
TiO_2 nanostructures	electrical	50	40	1	RT	1	n.a.	n.a.	28
PdPt film	electrical	4	5	10	150	10	n.a.	n.a.	29
Pt NW	electrical	100	-	1	25	1	n.a.	n.a.	30
Pd NRb	electrical	4	9	100	RT	20000	n.a.	n.a.	31
PdY film	optical	6	8	40	RT	1000	n.a.	n.a.	32
PdMg film	electrical	1	60	4000	100	-	n.a.	n.a.	33
Au@Pd NP	electrical	15	18	200	RT	1000	n.a.	n.a.	34
Pt@Pd NW	electrical	2	2.5	40	103	4000	n.a.	n.a.	35
polyurethane@Pd	electrical	24	-	1	RT	20	n.a.	n.a.	36
Pt@Pd/graphene	electrical	180	72	10	RT	1	n.a.	n.a.	37
Pd NP/graphene @PMMA	electrical	108	330	20	RT	250	n.a.	CH_4, CO, NO_2	38
Pd NP/TiO_2 NT	electrical	120	90	10	RT	-	n.a.	n.a.	39
Pd NW	electrical	25	-	1	RT	50	n.a.	n.a.	40
Pd/SiO_2/Au	optical	3	10	40	RT	5000	n.a.	n.a.	41

Active Element[a]	Transducing Method	t_{90} (s)	t_{10} (s)	Pressure (mbar)	Temperature (^{o}C)	LoD (ppm)	Hysteretic Behaviour[b]	Resistance to Poisoning Gases[b]	Ref
PdAu film	optical	15	15	20	RT	5000	hysteresis-free	CH_4	42
Pd NP/graphene	electrical	300	-	1	RT	20	n.a.	n.a.	43
PdNi NG	electrical	0.5	0.5	20	RT	500	n.a.	n.a.	44
Pd NG	electrical	5	200	40	RT	5000	n.a.	n.a.	45
Pd NW	electrical	4	-	24	RT	1000	n.a.	n.a.	46
Pd/Au film	optical	4.5	13	40	RT	-	n.a.	n.a.	47
Pd NG	electrical	498	3000	30	RT	20000	n.a.	n.a.	48
Pd NG	electrical	0.07	-	20	RT	25	n.a.	n.a.	49
Pd film	optical	10	-	40	RT	-	n.a.	n.a.	50
Pd microcantilever	mechanical	90	300	10	RT	-	n.a.	n.a.	51
fractured Pd NW	electrical	0.07	-	40	RT	10000	n.a.	CH_4	52,53

[a]NC = nanocube, NCf = nanocauliflower, NF = nanofiber, NG = nanogap, NP = nanoparticle, NR = nanorod, NRb = nanoribbon, NT = nanotube, NW = nanowire. [b]Pressure/temperature for response and recovery times measurements. [c]n.a. = not addressed.

References

(1) Nugroho, F. A. A.; Darmadi, I.; Zhdanov, V. P.; Langhammer, C. Universal Scaling and Design Rules of Hydrogen-Induced Optical Properties in Pd and Pd-Alloy Nanoparticles. *ACS Nano* **2018**, *12*, 9903–9912.

(2) Sauerbrey, G. Verwendung von Schwingquarzen Zur Wägung Dünner Schichten Und Zur Mikrowägung. *Zeitschrift für Phys.* **1959**, *155*, 206–222.

(3) Galipaud, J.; Martin, M. H.; Roué, L.; Guay, D. Pulsed Laser Deposition of PdCuAu Alloy Membranes for Hydrogen Absorption Study. *J. Phys. Chem. C* **2015**, *119*, 26451–26458.

(4) *ISO 26142:2010 Hydrogen Detection Apparatus - Stationary Applications*; 2010.

(5) Nugroho, F. A. A.; Darmadi, I.; Cusinato, L.; Susarrey-Arce, A.; Schreuders, H.; Bannenberg, L. J.; da Silva Fanta, A. B.; Kadkhodazadeh, S.; Wagner, J. B.; Antosiewicz, T. J.; *et al.* Metal–polymer Hybrid Nanomaterials for Plasmonic Ultrafast Hydrogen Detection. *Nat. Mater.* **2019**, *18*, 489–495.

(6) Cho, S. Y.; Ahn, H.; Park, K.; Choi, J.; Kang, H.; Jung, H. T. Ultrasmall Grained Pd Nanopattern H2Sensor. *ACS Sensors* **2018**, *3*, 1876–1883.

(7) He, J.; Villa, N. S.; Luo, Z.; An, S.; Shen, Q.; Tao, P.; Song, C.; Wu, J.; Deng, T.; Shang, W. Integrating Plasmonic Nanostructures with Natural Photonic Architectures in Pd-Modified *Morpho* Butterfly Wings for Sensitive Hydrogen Gas Sensing. *RSC Adv.* **2018**, *8*, 32395–32400.

(8) Hu, J.; Sun, Y.; Xue, Y.; Zhang, M.; Li, P.; Lian, K.; Zhuiykov, S.; Zhang, W.; Chen, Y. Highly Sensitive and Ultra-Fast Gas Sensor Based on CeO2-Loaded In2O3 Hollow Spheres for Ppb-Level Hydrogen Detection. *Sensors Actuators B Chem.* **2018**, *257*, 124–135.

(9) Lupan, O.; Postica, V.; Labat, F.; Ciofini, I.; Pauporté, T.; Adelung, R. Ultra-Sensitive and Selective Hydrogen Nanosensor with Fast Response at Room Temperature Based on a Single Pd/ZnO Nanowire. *Sensors Actuators B Chem.* **2018**, *254*, 1259–1270.

(10) Seo, J.; Lim, Y.; Shin, H. Self-Heating Hydrogen Gas Sensor Based on an Array of Single Suspended Carbon Nanowires Functionalized with Palladium Nanoparticles. *Sensors Actuators B Chem.* **2017**, *247*, 564–572.

(11) Zhang, D.; Sun, Y.; Jiang, C.; Zhang, Y. Room Temperature Hydrogen Gas Sensor Based on Palladium Decorated Tin Oxide/Molybdenum Disulfide Ternary Hybrid via Hydrothermal Route. *Sensors Actuators B Chem.* **2017**, *242*, 15–24.

(12) Luo, X.; You, K.; Hu, Y.; Yang, S.; Pan, X.; Wang, Z.; Chen, W.; Gu, H. Rapid Hydrogen Sensing Response and Aging of α-MoO3 Nanowires Paper Sensor. *Int. J. Hydrogen Energy* **2017**, *42*, 8399–8405.

(13) Sanger, A.; Jain, P. K.; Mishra, Y. K.; Chandra, R. Palladium Decorated Silicon Carbide Nanocauliflowers for Hydrogen Gas Sensing Application. *Sensors Actuators B Chem.* **2017**, *242*, 694–699.

(14) Shim, Y.-S.; Jang, B.; Suh, J. M.; Noh, M. S.; Kim, S.; Han, S. D.; Song, Y. G.; Kim,

D. H.; Kang, C.-Y.; Jang, H. W.; *et al.* Nanogap-Controlled Pd Coating for Hydrogen Sensitive Switches and Hydrogen Sensors. *Sensors Actuators B Chem.* **2018**, *255*, 1841–1848.

(15) Jang, J.-S.; Qiao, S.; Choi, S.-J.; Jha, G.; Ogata, A. F.; Koo, W.-T.; Kim, D.-H.; Kim, I.-D.; Penner, R. M. Hollow Pd–Ag Composite Nanowires for Fast Responding and Transparent Hydrogen Sensors. *ACS Appl. Mater. Interfaces* **2017**, *9*, 39464–39474.

(16) Yamazaki, H.; Hayashi, Y.; Masunishi, K.; Ono, D.; Ikehashi, T. High Sensitivity MEMS Capacitive Hydrogen Sensor with Inverted T-Shaped Electrode and Ring-Shaped Palladium Alloy for Fast Response and Low Power Consumption. *J. Micromechanics Microengineering* **2018**, *28*, 094001.

(17) Zhang, H.; Yi, J.; Jiang, X. Fast Response, Highly Sensitive and Selective Mixed-Potential H_2 Sensor Based on (La, Sr)(Cr, Fe)$O_{3-\delta}$ Perovskite Sensing Electrode. *ACS Appl. Mater. Interfaces* **2017**, *9*, 17218–17225.

(18) Woo, J.-A.; Phan, D.-T.; Jung, Y. W.; Jeon, K.-J. Fast Response of Hydrogen Sensor Using Palladium Nanocube-TiO2 Nanofiber Composites. *Int. J. Hydrogen Energy* **2017**, *42*, 18754–18761.

(19) Agrawal, A. V.; Kumar, R.; Venkatesan, S.; Zakhidov, A.; Zhu, Z.; Bao, J.; Kumar, M.; Kumar, M. Fast Detection and Low Power Hydrogen Sensor Using Edge-Oriented Vertically Aligned 3-D Network of MoS_2 Flakes at Room Temperature. *Appl. Phys. Lett.* **2017**, *111*, 093102.

(20) Hassan, K.; Chung, G.-S. Fast and Reversible Hydrogen Sensing Properties of Pd-Capped Mg Ultra-Thin Films Modified by Hydrophobic Alumina Substrates. *Sensors Actuators B Chem.* **2017**, *242*, 450–460.

(21) Kumar, M.; Kumar, R.; Rajamani, S.; Ranwa, S.; Fanetti, M.; Valant, M.; Kumar, M. Efficient Room Temperature Hydrogen Sensor Based on UV-Activated ZnO Nano-Network. *Nanotechnology* **2017**, *28*, 365502.

(22) Koo, W.-T.; Qiao, S.; Ogata, A. F.; Jha, G.; Jang, J.-S.; Chen, V. T.; Kim, I.-D.; Penner, R. M. Accelerating Palladium Nanowire H2 Sensors Using Engineered Nanofiltration. *ACS Nano* **2017**, *11*, 9276–9285.

(23) Hassan, K.; Uddin, A. S. M. I.; Ullah, F.; Kim, Y. S.; Chung, G.-S. Platinum/Palladium Bimetallic Ultra-Thin Film Decorated on a One-Dimensional ZnO Nanorods Array for Use as Fast Response Flexible Hydrogen Sensor. *Mater. Lett.* **2016**, *176*, 232–236.

(24) Moon, J.; Hedman, H.-P.; Kemell, M.; Tuominen, A.; Punkkinen, R. Hydrogen Sensor of Pd-Decorated Tubular TiO2 Layer Prepared by Anodization with Patterned Electrodes on SiO2/Si Substrate. *Sensors Actuators B Chem.* **2016**, *222*, 190–197.

(25) Sanger, A.; Kumar, A.; Kumar, A.; Chandra, R. Highly Sensitive and Selective Hydrogen Gas Sensor Using Sputtered Grown Pd Decorated MnO2 Nanowalls. *Sensors Actuators B Chem.* **2016**, *234*, 8–14.

(26) Chen, W. P.; Xiong, Y.; Li, Y. S.; Cui, P.; Guo, S. S.; Chen, W.; Tang, Z. L.; Yan, Z.; Zhang, Z. Extraordinary Room-Temperature Hydrogen Sensing Capabilities of Porous Bulk Pt–TiO2 Nanocomposite Ceramics. *Int. J. Hydrogen Energy* **2016**, *41*, 3307–3312.

(27) Uddin, A. S. M. I.; Chung, G.-S. A Self-Powered Active Hydrogen Gas Sensor with Fast Response at Room Temperature Based on Triboelectric Effect. *Sensors Actuators B Chem.* **2016**, *231*, 601–608.

(28) Xia, X.; Wu, W.; Wang, Z.; Bao, Y.; Huang, Z.; Gao, Y. A Hydrogen Sensor Based on Orientation Aligned TiO2 Thin Films with Low Concentration Detecting Limit and Short Response Time. *Sensors Actuators B Chem.* **2016**, *234*, 192–200.

(29) Hassan, K.; Iftekhar Uddin, A. S. .; Chung, G.-S. Fast-Response Hydrogen Sensors Based on Discrete Pt/Pd Bimetallic Ultra-Thin Films. *Sensors Actuators B Chem.* **2016**, *234*, 435–445.

(30) Yoo, H.-W.; Cho, S.-Y.; Jeon, H.-J.; Jung, H.-T. Well-Defined and High Resolution Pt Nanowire Arrays for a High Performance Hydrogen Sensor by a Surface Scattering Phenomenon. *Anal. Chem.* **2015**, *87*, 1480–1484.

(31) Pak, Y.; Lim, N.; Kumaresan, Y.; Lee, R.; Kim, K.; Kim, T. H.; Kim, S.-M.; Kim, J. T.; Lee, H.; Ham, M.-H.; *et al.* Palladium Nanoribbon Array for Fast Hydrogen Gas Sensing with Ultrahigh Sensitivity. *Adv. Mater.* **2015**, *27*, 6945–6952.

(32) Song, H.; Chen, Y.; Zhang, G.; Liu, Y.; Huang, P.; Zhao, H.; Yang, M.; Dai, J.; Li, Z. Optical Fiber Hydrogen Sensor Based on an Annealing-Stimulated Pd–Y Thin Film. *Sensors Actuators B Chem.* **2015**, *216*, 11–16.

(33) Sanger, A.; Kumar, A.; Chauhan, S.; Gautam, Y. K.; Chandra, R. Fast and Reversible Hydrogen Sensing Properties of Pd/Mg Thin Film Modified by Hydrophobic Porous Silicon Substrate. *Sensors Actuators B Chem.* **2015**, *213*, 252–260.

(34) Rajoua, K.; Baklouti, L.; Favier, F. Electronic and Mechanical Antagonist Effects in Resistive Hydrogen Sensors Based on Pd@Au Core–Shell Nanoparticle Assemblies Prepared by Langmuir–Blodgett. *J. Phys. Chem. C* **2015**, *119*, 10130–10139.

(35) Li, X.; Liu, Y.; Hemminger, J. C.; Penner, R. M. Catalytically Activated Palladium@Platinum Nanowires for Accelerated Hydrogen Gas Detection. *ACS Nano* **2015**, *9*, 3215–3225.

(36) Chen, R.; Ruan, X.; Liu, W.; Stefanini, C. A Reliable and Fast Hydrogen Gas Leakage Detector Based on Irreversible Cracking of Decorated Palladium Nanolayer upon Aligned Polymer Fibers. *Int. J. Hydrogen Energy* **2015**, *40*, 746–751.

(37) Phan, D.-T.; Uddin, A. S. M. I.; Chung, G.-S. A Large Detectable-Range, High-Response and Fast-Response Resistivity Hydrogen Sensor Based on Pt/Pd Core–shell Hybrid with Graphene. *Sensors Actuators B Chem.* **2015**, *220*, 962–967.

(38) Hong, J.; Lee, S.; Seo, J.; Pyo, S.; Kim, J.; Lee, T. A Highly Sensitive Hydrogen Sensor with Gas Selectivity Using a PMMA Membrane-Coated Pd Nanoparticle/Single-Layer Graphene Hybrid. *ACS Appl. Mater. Interfaces* **2015**, *7*, 3554–3561.

(39) Xiang, C.; She, Z.; Zou, Y.; Cheng, J.; Chu, H.; Qiu, S.; Zhang, H.; Sun, L.; Xu, F. A Room-Temperature Hydrogen Sensor Based on Pd Nanoparticles Doped TiO2 Nanotubes. *Ceram. Int.* **2014**, *40*, 16343–16348.

(40) Lim, S. H.; Radha, B.; Chan, J. Y.; Saifullah, M. S. M.; Kulkarni, G. U.; Ho, G. W. Flexible Palladium-Based H_2 Sensor with Fast Response and Low Leakage Detection

by Nanoimprint Lithography. *ACS Appl. Mater. Interfaces* **2013**, *5*, 7274–7281.

(41) Perrotton, C.; Westerwaal, R. J.; Javahiraly, N.; Slaman, M.; Schreuders, H.; Dam, B.; Meyrueis, P. A Reliable, Sensitive and Fast Optical Fiber Hydrogen Sensor Based on Surface Plasmon Resonance. *Opt. Express* **2013**, *21*, 382.

(42) Westerwaal, R. J.; Rooijmans, J. S. A.; Leclercq, L.; Gheorghe, D. G.; Radeva, T.; Mooij, L.; Mak, T.; Polak, L.; Slaman, M.; Dam, B.; *et al.* Nanostructured Pd–Au Based Fiber Optic Sensors for Probing Hydrogen Concentrations in Gas Mixtures. *Int. J. Hydrogen Energy* **2013**, *38*, 4201–4212.

(43) Chung, M. G.; Kim, D.-H.; Seo, D. K.; Kim, T.; Im, H. U.; Lee, H. M.; Yoo, J.-B.; Hong, S.-H.; Kang, T. J.; Kim, Y. H. Flexible Hydrogen Sensors Using Graphene with Palladium Nanoparticle Decoration. *Sensors Actuators B Chem.* **2012**, *169*, 387–392.

(44) Lee, J.; Shim, W.; Lee, E.; Noh, J.-S.; Lee, W. Highly Mobile Palladium Thin Films on an Elastomeric Substrate: Nanogap-Based Hydrogen Gas Sensors. *Angew. Chemie Int. Ed.* **2011**, *50*, 5301–5305.

(45) Kiefer, T.; Villanueva, L. G.; Fargier, F.; Favier, F.; Brugger, J. Fast and Robust Hydrogen Sensors Based on Discontinuous Palladium Films on Polyimide, Fabricated on a Wafer Scale. *Nanotechnology* **2010**, *21*, 505501.

(46) Offermans, P.; Tong, H. D.; van Rijn, C. J. M.; Merken, P.; Brongersma, S. H.; Crego-Calama, M. Ultralow-Power Hydrogen Sensing with Single Palladium Nanowires. *Appl. Phys. Lett.* **2009**, *94*, 223110.

(47) Monzón-Hernández, D.; Luna-Moreno, D.; Martínez-Escobar, D. Fast Response Fiber Optic Hydrogen Sensor Based on Palladium and Gold Nano-Layers. *Sensors Actuators B Chem.* **2009**, *136*, 562–566.

(48) Kiefer, T.; Favier, F.; Vazquez-Mena, O.; Villanueva, G.; Brugger, J. A Single Nanotrench in a Palladium Microwire for Hydrogen Detection. *Nanotechnology* **2008**, *19*, 125502.

(49) Xu, T.; Zach, M. P.; Xiao, Z. L.; Rosenmann, D.; Welp, U.; Kwok, W. K.; Crabtree, G. W. Self-Assembled Monolayer-Enhanced Hydrogen Sensing with Ultrathin Palladium Films. *Appl. Phys. Lett.* **2005**, *86*, 1–3.

(50) Villatoro, J.; Monzón-Hernández, D. Fast Detection of Hydrogen with Nano Fiber Tapers Coated with Ultra Thin Palladium Layers. *Opt. Express* **2005**, *13*, 5087.

(51) Baselt, D. R.; Fruhberger, B.; Klaassen, E.; Cemalovic, S.; Britton, C. L.; Patel, S. V.; Mlsna, T. E.; McCorkle, D.; Warmack, B. Design and Performance of a Microcantilever-Based Hydrogen Sensor. *Sensors Actuators B Chem.* **2003**, *88*, 120–131.

(52) Favier, F.; Walter, E. C.; Zach, M. P.; Benter, T.; Penner, R. M. Hydrogen Sensors and Switches from Electrodeposited Palladium Mesowire Arrays. *Science (80-.).* **2001**, *293*, 2227–2231.

(53) Walter, E. C.; Favier, F.; Penner, R. M. Palladium Mesowire Arrays for Fast Hydrogen Sensors and Hydrogen-Actuated Switches. *Anal. Chem.* **2002**, *74*, 1546–1553.